Molecular Crystals and Liquid Crystals Science and Technology. Section A. Molecular Crystals and Liquid Crystals

Publication details, including instructions for authors and subscription information:
http://www.tandfonline.com/loi/gmcl19

Paranematic-Nematic Phase Transition of a Liquid Crystal Confined to a Controlled Porous Glass

A. Zidansek [a b d], S. Kralj [b], G. Lahajnar [b], S. Žumer [b c] & R. Blinc [b c]

[a] Montana State University, Department of Physics and Department of Chemistry, Bozeman, MT, 59717, USA

[b] J.Stefan Institute, University of Ljubljana, Jamova 39, 1000, Ljubljana, Slovenia

[c] Department of Physics, FMF, University of Ljubljana, Jadranska 19, 1000, Ljubljana, Slovenia

[d] J. Stefan Institute, University of Ljubljana, Jamova 39, 1000, Ljubljana, Slovenia

Version of record first published: 04 Oct 2006

To cite this article: A. Zidansek, S. Kralj, G. Lahajnar, S. Žumer & R. Blinc (1997): Paranematic-Nematic Phase Transition of a Liquid Crystal Confined to a Controlled Porous Glass, Molecular Crystals and Liquid Crystals Science and Technology. Section A. Molecular Crystals and Liquid Crystals, 299:1, 307-320

To link to this article: http://dx.doi.org/10.1080/10587259708042009

Mol. Cryst. Liq. Cryst., 1997, Vol. 299, pp. 307–320
Reprints available directly from the publisher
Photocopying permitted by license only

PARANEMATIC-NEMATIC PHASE TRANSITION OF A LIQUID CRYSTAL CONFINED TO A CONTROLLED POROUS GLASS

ALEKSANDER ZIDANŠEK[1,2*], SAMO KRALJ[2], GOJMIR LAHAJNAR[2], SLOBODAN ŽUMER[2,3], AND ROBERT BLINC[2,3]

[1]Montana State University, Department of Physics and Department of Chemistry, Bozeman, MT 59717, USA

[2]J. Stefan Institute, University of Ljubljana, Jamova 39, 1000 Ljubljana, Slovenia

[3]Department of Physics, FMF, University of Ljubljana, Jadranska 19, 1000 Ljubljana, Slovenia

*Current address: J. Stefan Institute, University of Ljubljana, Jamova 39, 1000 Ljubljana, Slovenia

Abstract A deuteron NMR study of a pentylcyanobiphenil (5CB) liquid crystal confined in controlled pore glass (CPG) matrices of different pore diameters 2R between 7 nm and 400 nm has been performed. The paranematic-nematic (P-N) phase transition seems to be gradual in pores with $2R \leq 24$ nm and discontinuous in larger pores. Possible reasons for the observed temperature shift ΔT and qualitative change of the phase transition are analyzed using a simple phenomenological approach. The theoretical analysis suggests that both surface interaction and elastic distortions significantly influence the $\Delta T = \Delta T(R)$ dependence obtained in CPG samples.

INTRODUCTION

Recently many studies have been devoted to the behavior of liquid crystals (LC) confined to different porous materials[1] (e.q. aerogels[2-5], CPG[6,7], Vycor[8] glass, and other porous glasses[9]). In such systems the typical size of a void containing LC is below 1μm and different voids are in most cases strongly interconnected. Thus finite size effects, geometrically induced randomness, defects, and surface interactions play in general an important role.

In this work we report on a deuteron NMR lineshape study of a pentyl-cyanobiphenil (5CB) liquid crystal confined to different controlled porous glass (CPG) matrices. The CPG matrices[6,7] consist of strongly interconnected voids. The voids are strongly curved and have locally cylinder like symmetry with a relatively small variation of the radius. The void surface is relatively smooth on the nm scale. In our previous publication[7] on this subject we explained the measured NMR-line shapes, hysteresis effects and qualitatively discussed possible reasons for the change of the character of the paranematic-nematic (P-N) phase transition. The paranematic[10] phase has a weak but finite degree of nematic ordering due to the local surface ordering effect. In this work we focus on the dependence of the P-N transition on the CPG voids' diameter. Quantitative estimates are made using the Landau-de Gennes approach.

EXPERIMENTAL RESULTS

We studied CPG matrices with average pore diameters 2R of 7.4 nm, 24 nm, 50 nm, 100 nm, 140 nm, 300 nm and 400 nm, and a very narrow monodispersed pore size distribution with the width of $\sim 10\%$ around the average pore

diameter.[7] The immersed liquid crystal 5CB was deuterated at the βd_2 position. The deuteron NMR spectra were recorded at resonance frequencies of 58.37 MHz and 30.6 MHz. A $(\pi/2)_x$-$(\pi/2)_y$ pulse sequence with phase cycling was used to obtain NMR spectra in the nematic phase.

The temperature dependence of the average nematic ordering for some pore sizes is presented in Fig.1. The degree of ordering was inferred from the measured line shapes. Details are given in ref.(7). In the samples with $R \leq 24$nm the P-N transition seems to be gradual and for larger radia discontinuous. In the inset to Fig.1 the shift of the P-N phase transition is depicted as a function of R. Data suggest that the temperature shift scales approximately as $1/R^{1.3}$.

THEORETICAL CONSIDERATIONS

Free energy

In the following we analyze theoretically the influence of different mechanisms on the character and temperature shift of the paranematic-nematic phase transition of a LC confined to a cavity of a general shape. We use the phenomenological continuum description where nematic ordering is expressed in terms of the nematic director field $\vec{n}$ and the uniaxial nematic order parameter S. In this case the free energy F is expressed as[11,12]

$$F = \int_{\text{volume}} d^3\vec{r} \left(a(T-T_*)S^2 - bS^3 + cS^4 + \tfrac{1}{2}\left[K_{11}(\text{div}\vec{n})^2 + K_{22}(\vec{n}.\text{curl}\vec{n})^2 + K_{33}(\vec{n}\times\text{curl}\vec{n})^2 \right] \right.$$
$$\left. - \frac{K_{24}}{2}\,\text{div}(\vec{n}\times\text{curl}\vec{n}+\vec{n}\,\text{div}\vec{n}) + \tfrac{1}{2}\, l_0(\text{grad}S)^2 - \frac{\Delta\chi S B^2}{2\mu_0}(\vec{n}.\vec{e}_f)^2 \right) +$$
$$+ \int_{\text{surface}} d^2\vec{r} \left(W_2 w_2(\vec{n})\, S^2 - W_1 w_1(\vec{n})\, S \right). \qquad (1)$$

Here a, b, c, T_* are material constants. The elastic properties of LC are

determined by elastic constants K_i (i=11,22,33,24) and l_o. The surface-LC interaction strength is given by constants W_1 and W_2. The orientational dependence of the surface interaction[13] is given by dimensionless functions $w_1(\vec{n})$ and $w_2(\vec{n})$. We define them in such a way that in the strong anchoring regime it holds $w_1=w_2=1$. It is to be stressed that in the expression (1) only the most important terms are included that reproduce the main qualitative and quantitative features observed in the samples studied[11,12].

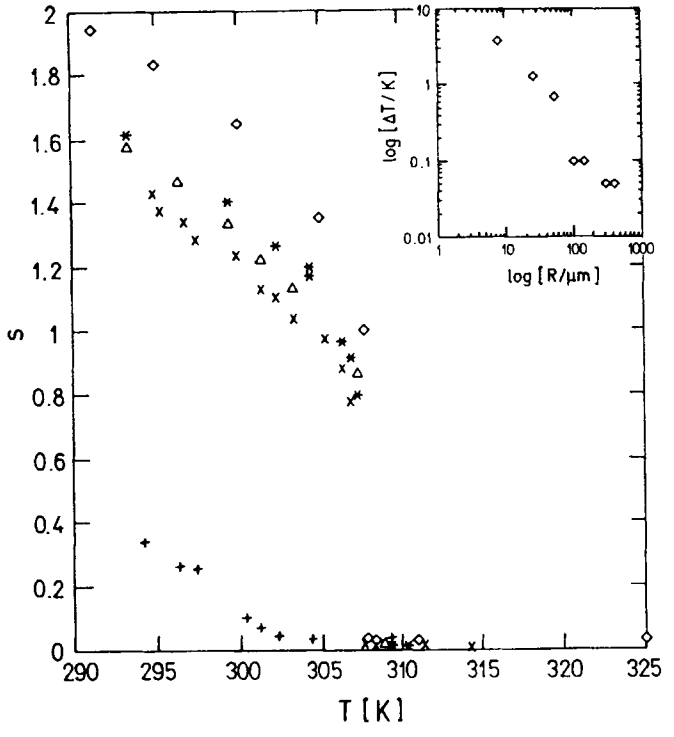

FIGURE 1 The effective scaled nematic order parameter $s=S_{eff}/S_o$ as function of temperature for 2R=7 (+), 50 (x), 100 (Δ), and 140 (*), obtained from the deuteron NMR linewidth. For comparison the bulk data are also plotted (◊). In the inset the log-log dependence of the phase temperature shift as a function of R is shown. S_o is the value of the order parameter at the nematic-isotropic transition of the bulk LC.

Character and shift of the P-N phase transition

We employ the following approximations: (i) "Direct" coupling between $\vec{n}$ and S is neglected. Thus in the model we calculate the $\vec{n}$ profile and based on it evaluate the effective order parameter S_{eff} within the sample. (ii) We assume that in most of the sample the order parameter is constant and close to S_{eff}. The orientational ordering recovers to its average value on the correlation length (ξ) scale. i.e. at defect sites $|\mathrm{grad}(S_{eff})| \approx S_{eff}/\xi$. (iii) The S_{eff} (i.e. temperature) dependence of elastic constants is approximately expressed[12,14] as $K_{24}=k_{24}^{(1)}S_{eff}+k_{24}^{(2)}S_{eff}^2$, $K_{11}=k_1S_{eff}^2$, $K_{22}=k_2S_{eff}^2$, $K_{33}=k_3S_{eff}^2$. Here k_i (i=1,2,3,24) and l_o are assumed to be temperature independent. (iv) The confining worm-like void resembles a cylinder with radius R.

We further introduce the dimensionless coordinate system $\vec{x}$ measured in units of R, the dimensionless operators $\nabla.=R$ div, $\nabla x=R$ curl, $\nabla=R$ grad and the scaled effective nematic order parameter $s=S_{eff}/S_o$. Here $S_o=b/(2c)$ describes the value of the order parameter at the I-N phase transition at $T=T_{NI}$ in the bulk. We introduce the dimensionless temperature $t=(T-T_*)/(T_{NI}-T_*)$, the dimensionless elastic constants a_i (i=22,33,24) measured in units of $K_{11}(T=T_{NI})$: $a_2=k_2/k_1$, $a_3=k_3/k_1$, $a_{24}^{(1)}=k_{24}^{(1)}/(k_1S_o)$, $a_{24}^{(2)}=k_{24}^{(2)}/k_1$. The important characteristic[11] lengths, expressed at $T=T_{NI}$, entering the model are the nematic correlation length $\xi^2=a(T_{NI}-T_*)/l_o$, the external field correlation length $\xi_f^2=\Delta\chi S_oB^2/(k_1S_o^2\mu_o)$, and the surface extrapolation lengths $d_1=k_1S_o^2/(W_1S_o)$, $d_2=k_2S_o^2/(W_2S_o^2)$.

Taking this into in account we express the dimensionless free energy as[4,15]

$$G = s^2\, t_{ef} - 2\, s^3 + s^4 - h\, s. \qquad (2)$$

The quantities t_{ef} and h play the role of an effective temperature and an

effective square external field:

$$t_{ef} = t + \frac{k_1}{l_o}\left(G_e \frac{\xi^2}{R^2} - a_{24}^{(2)} G_{24} \frac{\xi^2}{R^2} + G_2 \frac{\xi^2}{Rd_2} \right) + t_{def}\,, \tag{3a}$$

$$h = \frac{k_1}{l_o}\left(G_f \frac{\xi^2}{\xi_f^2} + a_{24}^{(1)} G_{24} \frac{\xi^2}{R^2} + G_1 \frac{\xi^2}{Rd_1} \right). \tag{3b}$$

The quantity t_{def} describes the contribution of the defects. For point defect it roughly holds $t_{def} \approx \frac{N_{def}}{2V} \frac{\xi^3}{R^3}$ and for line defect $t_{def} \approx \frac{N_{def}}{2V} \frac{\xi^2}{R^2}$, where N_{def} is the number of defects and $V = \int d^3\vec{x}$. The value of t_{ef} and h is influenced by the nematic director field structure which enters the integrals G_i (i=1,2,24,e,f) defined in eqs.(4). The separation of the R dependence in t_{ef} and h into the explicit and implicit parts (via integrals G_i) is convenient because the G_i in many cases depend weakly on R. The integrals entering eqs.(3) are defined as

$$G_e = \frac{1}{V} \int_{volume} d^3\vec{x}\, \frac{1}{2}\left((\nabla.\vec{n})^2 + a_{22}(\vec{n}.\nabla x\vec{n})^2 + a_{33}(\vec{n}x\nabla x\vec{n})^2 \right), \tag{4a}$$

$$G_f = \frac{1}{V} \int_{volume} d^3\vec{x}\, \frac{1}{2} (\vec{n}.\vec{e}_f)^2\,, \tag{4b}$$

$$G_{24} = \frac{1}{V} \int_{volume} d^3\vec{x}\, \frac{1}{2} \nabla.(\vec{n}x\nabla x\vec{n} + \vec{n}\,\nabla.\vec{n}) = \frac{1}{V} \int_{surface} d^2\vec{x}\, \frac{1}{2} (\vec{n}x\nabla x\vec{n} + \vec{n}\,\nabla.\vec{n}).\vec{\nu}\,, \tag{4c}$$

$$G_1 = \frac{1}{V} \int_{surface} d^2\vec{x}\, w_1(\vec{n}),\quad G_2 = \frac{1}{V} \int_{surface} d^2\vec{x}\, w_2(\vec{n})\,, \tag{4d}$$

where $\vec{\nu}$ defines a local orientation of a void surface normal. The director field is obtained as a solution of Euler-Lagrange equations for $\vec{n}$ assuming that variations of $\vec{n}$ and s are decoupled. A value of the scalar effective order parameter s is then obtained from the minimization of G, i.e. by solving the equation $\frac{\partial G}{\partial s}=0$. The solutions for different values of h are given in Fig.2.

For $h \le h_C \equiv 0.5$ the P-N transition (I-N for h=0) is discontinuous and becomes gradual for $h \ge h_C$. In the regime $h<h_C$ the phase transition takes place

at $(t_{ef})_{PT}=1+h$. The corresponding actual dimensionless transition temperature t related to t_{ef} by eq.(3a) has at the transition point the following value:

$$t_{PT} = 1 - t_{def} + \frac{k_1}{l_0}\left(- G_e \frac{\xi^2}{R^2} + G_f \frac{\xi^2}{\xi_f^2} + (a_{24}^{(1)}+a_{24}^{(2)})\, G_{24} \frac{\xi^2}{R^2} - G_2 \frac{\xi^2}{Rd_2} + G_1 \frac{\xi^2}{Rd_1}\right). \quad (5)$$

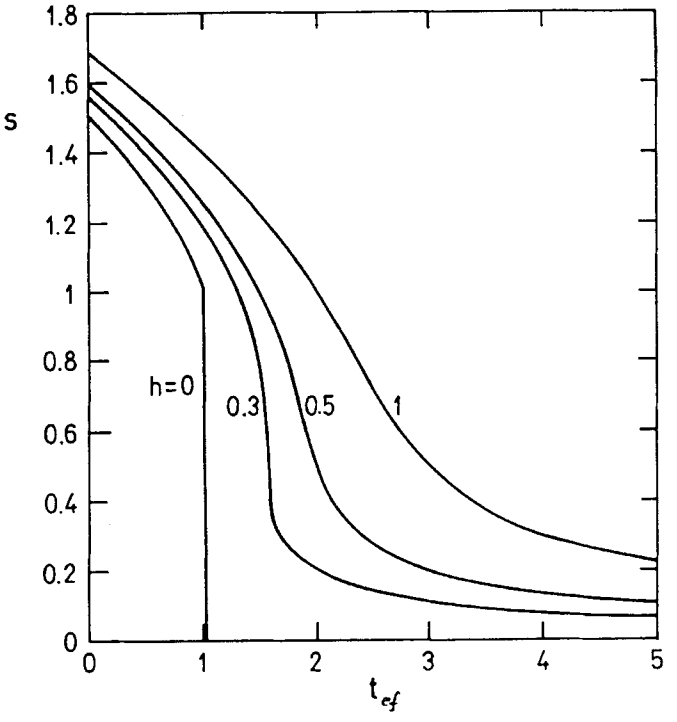

FIGURE 2 The average scaled nematic order parameter s as function of t_{ef} for different values of h. For $h<h_c \equiv 0.5$ the P-N transition is discontinuous and gradual for $h \geq h_c$.

In the undistorted bulk the transition takes place at $t_{PT}=1$. If $h>0$ and $h<h_c$ then the remaining terms in eq.(5) describe the shift ΔT of the transition temperature. The shift ΔT due to elastic distortion in $\vec{n}$ is proportional to $1/R^2$ in case that the integrals G_e weakly depend on R. This holds true if the structure within a cavity is scale invariant which is often realized in the strong

anchoring regime and negligible external field influence. On the other hand the shift due to variations in S at defects is proportional to $1/R^3$ for point defects and $1/R^2$ for line defects. The elastic distortions due to the bulk elastic constants depress the transition temperature. On the other hand the saddle splay elastic term[16] can provide shift in either direction depending on the sign of this constant. The external field contribution increases t_{PT}. This term depends on R only via the integral G_f. At least in the strong anchoring regime the surface interaction terms scale as 1/R. The W_1 contribution enhances while W_2 depresses t_{PT}.

The shift in the transition temperature becomes significant (comparable to 1) when the typical lengths of the system (R, d_1, d_2, ξ_f) are close to ξ. For most director structures the integrals G_i (i=1,2,24,e,f) typically range between 1 and 100. Characteristic lengths are typically of the order $\xi \approx 0.01\mu$m, d_1 and d_2 vary from 0.01μm to 1μm, ξ_f from 0.1μm to 1μm.

The character of the transition is in this picture controlled by the field h, defined in eq.(3b). The transition becomes gradual for $h \geq h_C \equiv 0.5$, which can be triggered either by the external field contribution, the saddle splay elastic constant K_{24} providing $G_{24}k_{24}^{(1)}>0$ or the W_1 surface interaction contribution if $\xi_f \approx \xi$ or $R \approx \xi$ or $Rd_1 \approx \xi^2$.

In order to test the validity of the approach we calculate the effective value of s for a spherical droplet having the radial director field in two different ways: (i) using the procedure described above ($s=s_1$) and (ii) taking into account $s(\vec{r})$ variation and performing the average over the droplet ($s=s_2=\frac{1}{V}\int s(\vec{x})d^3\vec{x}$). The relative departure $\Delta s/s$ as a function of R is shown in Fig.3 ($\Delta s=s_1-s_2$, $s=(s_1+s_2)/2$). The results indicate that the above approximation works quite well down to the limit $R/\xi=1$.

Model nematic structures

To illustrate the effect of various director structures on t_{PT} and h we chose some structures for which analytic solutions are known and mimic to some extent possible scenaria encountered in CPG. These structures[17] are the homogeneous (H), the escaped radial (ER), and the escaped radial with point defects (ERPD) which are conventionally realized in long cylinders. They are schematically shown in Fig.4. With the ERPD structure we simulate the influence of the concentration of defects on the phase transition. These appear in the real samples at the intersection of voids. A more detailed discussion of possible director fields in CPG samples is given in ref.7.

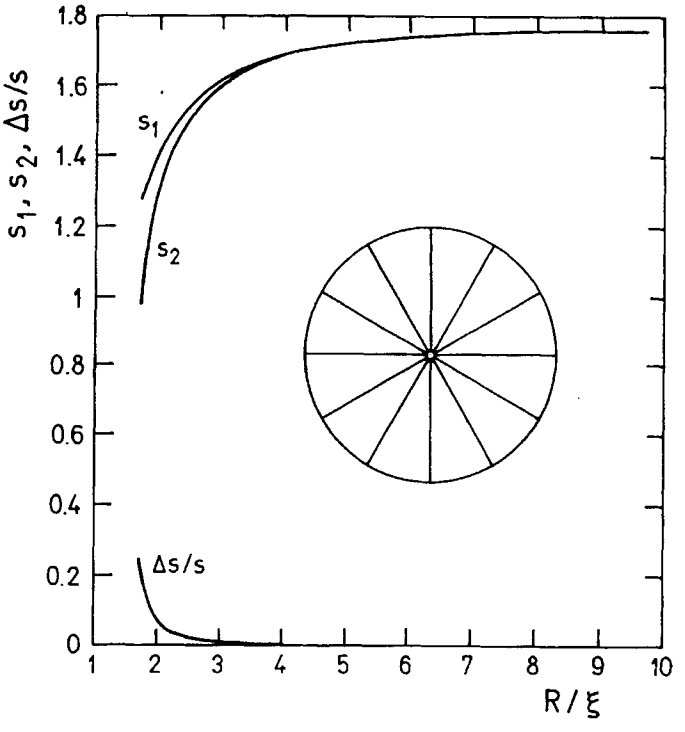

FIGURE 3 The relative departure $\Delta s/s$ as function of R. In the inset the radial director structure is plotted schematically. $\Delta s=s_1-s_2$, $s=(s_1+s_2)/2$

To evaluate integrals (4) for these structures we parametrize the director field as $\vec{n}=\sin\theta\ \vec{e}_z+\cos\theta\ \vec{e}_\rho$. Here $\vec{e}_z$ and $\vec{e}_\rho$ denote unit vectors along the cylinder axis and perpendicular to it. We further set $a_{33}=1$ (the a_{22} elastic term does not influence these structures), assume strong anchoring regime and neglect the external field contribution. In the H structure, which is realized in the case of planar anchoring or very weak homeotropic anchoring[17], $\theta=0$ everywhere. The ER (eq.(6a)) and ERPD (eq.(6b)) director profiles, that can be realized for the homeotropic anchoring, are given by

$$\theta = 2\ \mathrm{atan}(\rho), \tag{6a}$$

$$\theta = \mathrm{atan}\left(\frac{\rho}{z(1\text{-}z\ R/L)(1\text{-}\rho)}\right), \tag{6b}$$

where $\rho=1$ at the cylinder surface and L is the average distance between neighboring point defects lying on the cylinder axis. The relation (6a) is exact in the strong anchoring regime. The ansatz[17] (6b) works well for $L/R<4$ and strong anchoring.

For these structures the integrals G_i defined by eqs. (4) have simple forms so that the effective field h and the transition temperatures for $h \le h_C$ can be written as:

$$t_{PT}(H) = 1 + \left(-\frac{2\xi^2}{Rd_2} + \frac{2\xi^2}{Rd_1}\right)\frac{k_1}{l_o},\ h(H) = \frac{2\xi^2}{Rd_1}; \tag{7a}$$

$$t_{PT}(ER) = 1 + \left[-\frac{\xi^2}{R^2} - \frac{2\xi^2}{Rd_2} + \frac{2\xi^2}{Rd_1} + (a_{24}^{(1)}+a_{24}^{(2)})\frac{\xi^2}{R^2}\right]\frac{k_1}{l_o},$$

$$h(ER) = a_{24}^{(1)}\frac{\xi^2}{R^2} + \frac{2\xi^2}{Rd_1}; \tag{7b}$$

$$t_{PT}(ERPD)=1-\frac{\xi^3}{R^3}\left[-\left(3+\frac{8}{9}-\frac{4}{3}\log\left(\frac{L}{R}\right)+\frac{\pi}{5}\frac{L}{R}+\ldots\right)\frac{\xi^2}{R^2} - \frac{2\xi^2}{Rd_2} + \frac{2\xi^2}{Rd_1} + (a_{24}^{(1)}+a_{24}^{(2)})\frac{\xi^2}{R^2}\right]\frac{k_1}{l_o},$$

$$h(ERPD) = h(ER). \tag{7c}$$

In (7c) only the leading terms of the L/R expansion are taken into account. The t_{PT} and h dependence on R for different structures and typical values of material constants is shown in Fig.5.

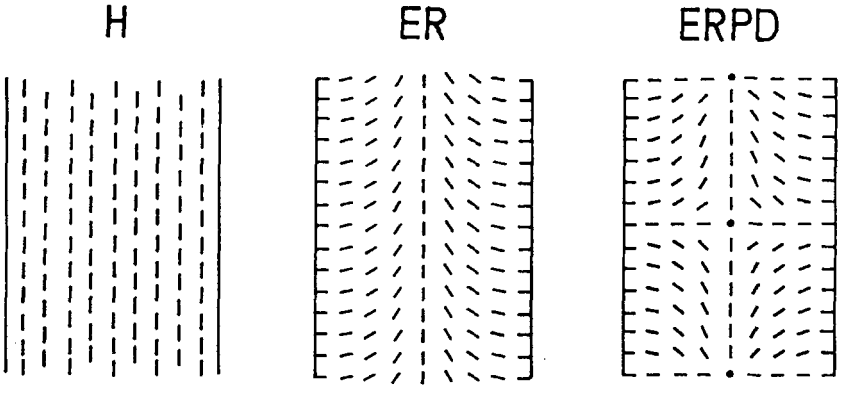

FIGURE 4 Schematic presentation of the H, ER and ERPD structure. In the H structure the director field is along the cylinder axis. In the ER structure $\vec{n}$ tends to be oriented radially at the cylinder surface and gradually escapes along the cylinder axis close to the center of the cylinder. The ERPD structure consists of partially escaped domains with alternating radial and hyperbolic point defects.

CONCLUSIONS

We have studied both experimentally and theoretically the temperature shift ΔT and the character of the P-N phase transition of the 5CB nematic liquid crystal confined to various CPG host matrices. Different CPG matrices are characterized by the average void radius R. The deuterium NMR absorption spectra reveal that in matrices with $2R \leq 24$ nm the transition seems to be gradual whereas it becomes discontinuous for matrices with $2R \geq 50$ nm. The phase transition temperature shift ΔT scales approximately as $1/R^{1.3}$.

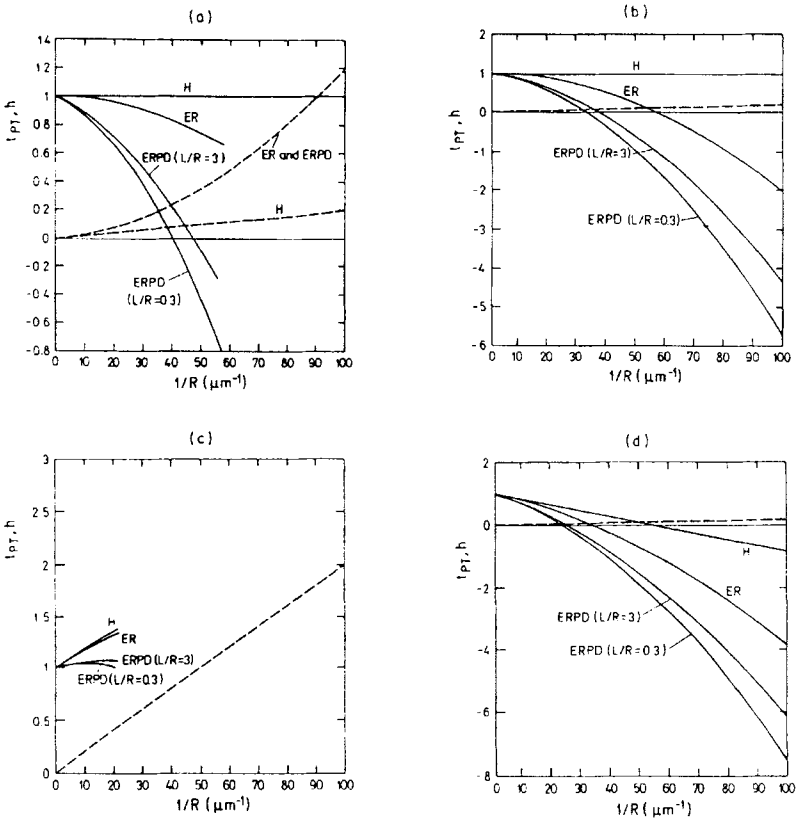

FIGURE 5 Dependence of t_{PT} (full line) and h (dashed line) on R for the H, ER and ERPD structure. In the case of ERPD structure cases of L/R=0.3 and L/R=3 are shown. The material constants are chosen: (a) $d_1=d_2=0.1\mu m$, $a_{24}^{(1)}=a_{24}^{(2)}=1$, (b) $d_1=d_2=0.1\mu m$, $a_{24}^{(1)}=a_{24}^{(2)}=0$, (c) $d_1=0.01\mu m$, $d_2=0.1\mu m$, $a_{24}^{(1)}=a_{24}^{(2)}=0$, (d) $d_1=0.1\mu m$, $d_2=0.01\mu m$, $a_{24}^{(1)}=a_{24}^{(2)}=0$. In all cases $k_1/l_0=1$, $1/\xi_f=0$. For cases b, c, d the h(R) dependence is the same for all the structures.

A theoretical analysis based on the Landau-de Gennes picture reveals that the ΔT due to elastic distortions in $\vec{n}$ in most cases approximately scales as $1/R^2$ and due to variations in S as $1/R^3$ for point defects and $1/R^2$ for line defects. The bulk elastic terms decrease ΔT while the saddle splay contribution can either increase or decrease it depending on the sign of K_{24}. The surface

interaction contributions scale as 1/R. The shift of transition temperature can become apparent when the relevant characteristic distances (d_1, d_2, ξ_f or R) becomes comparable to ξ.

Note that the cases demonstrated in Fig.5 only roughly mimic possible scenaria encountered in a real sample. Most of the structures analyzed correspond to the situation of strong homeotropic anchoring. However for small radia the bulk elasticity forces the system to arrange like in the case of planar anchoring (i.e., the geometry of the surface becomes dominant). This transition takes place when R/d_1 or R/d_2 are in the range between 1 to 10. But this transition can not relax most of the defects in the director field which are the consequence of randomly interconnected worm-like voids. The ERPD structure was chosen to emphasize the effect of concentration of defects on the phase behavior which is in our case only weakly influenced by the anchoring strength. On the other hand the K_{24} contribution strongly depends on anchoring conditions.

ACKNOWLEDGEMENTS

A. Zidanšek gratefully acknowledges the financial support of the Slovenian Scientific Foundation (Slovenska znanstvena fundacija, ZIT-0026-95) and International Institute of Education (Fulbright Program No. 33917). We thank T.J. Sluckin, I. Muševič and R. Stannarius for useful conversations and to M.M. Pintar and S.S. Keast for providing samples.

REFERENCES

1. Liquid Crystals in Complex Geometries formed by polymer and porous networks, eds. G.P.Crawford and S.Žumer, Taylor and Francis, 1996.
2. N.A. Clark, T. Bellini, R.M. Malzbender, B.N. Thomas, A.G. Rappaport,

C.D. Muzny, D.W. Schaefer, and L. Hrubesh, Phys.Rev.Lett., 71, 3505 (1993).

3. G. Schwalb, F.W. Deeg, Phys.Rev.Lett., 74, 1383 (1995).
4. A. Zidanšek, S. Kralj, G. Lahajnar, and R. Blinc, Phys.Rev.E, 51, 3332 (1995).
5. A. Mertelj, M. Čopič, accepted in Phys.Rev.E.
6. M.D. Dadmun and M. Muthukumar, J.Chem.Phys., 98, 4850 (1993).
7. S. Kralj, A. Zidanšek, G. Lahajnar, I. Muševič, S. Žumer, R. Blinc, and M.M. Pintar, Phys.Rev.E, 53, 3629 (1996).
8. G.S. Iannacchione, G.P. Crawford, S. Žumer, J.W. Doane, and D. Finotello, Phys.Rev.Lett., 71, 2595 (1993).
9. F.M. Aliev and M.N. Breganov, Zh.Eksp.Teor.Fiz., 95, 122 (1989) [Sov.Phys.JETP 68, 70 (1989)].
10. P.Sheng, Phys.Rev.A, 26, 1610 (1982).
11. P.G. de Gennes and J.Prost, The Physics of Liquid Crystals (Oxford University Press, Oxford, 1993).
12. E.B. Priestley, P.J. Wojtowitz, and P. Sheng, Introduction to Liquid Crystals (Plenum Press, New York and London, 1974), p.143.
13. G.Barbero, E.Miraldi, and A.Stepanescu, J.Appl.Phys., 68, 2063 (1990).
14. A.I. Alexe-Ionescu, G. Barbero, and G. Durand, J.Phys.II France, 3, 1247 (1993).
15. D.J. Cleaver, S. Kralj, T.J. Sluckin and M.P. Allen, Liquid Crystals in Complex Geometries formed by polymer and porous networks, eds. G.P.Crawford and S.Žumer, Taylor and Francis, 467 (1996).
16. V.M. Pergamenshchik, Phys.Rev. E, 48, 1254 (1993).
17. D.W. Allender, G.P. Crawford, and J.W. Doane, Phys.Rev.Lett., 67, 1442 (1991).